Journal of Materials Chemistry A

PAPER

View Article Online
View Journal | View Issue

Cite this: J. Mater. Chem. A, 2014, 2, 12068

In situ growth of monodisperse Fe_3O_4 nanoparticles on graphene as flexible paper for supercapacitor†

Miaomiao Liu and Jing Sun*

Received 27th March 2014
Accepted 1st June 2014

DOI: 10.1039/c4ta01442a

www.rsc.org/MaterialsA

A well-organized Fe_3O_4/graphene sheet composite (GS/Fe_3O_4) paper has been constructed *via* a universal three-step method. A graphene oxide/Fe_2O_3 composite (GO/Fe_2O_3) dispersion is prepared followed by vacuum filtration of the dispersion to obtain a GO/Fe_2O_3 composite paper. Finally, heat treatment of the GO/Fe_2O_3 paper produces the GS/Fe_3O_4 paper. Fe_3O_4 nanoparticles of ~5 nm are grown *in situ* and uniformly anchored on graphene sheets by covalent chemical bonding. The three-dimensional (3-D) conductive paper provides good electrical contact and improves the dispersion of well-adhered Fe_3O_4 nanoparticles, further boosting the accessible capacity. Therefore, the GS/Fe_3O_4 paper exhibits excellent rate performance and cyclic stability as a flexible anode material for supercapacitors. The optimized GS/Fe_3O_4 paper could achieve a high specific capacitance of 368 F g^{-1} at 1 A g^{-1} and remain 245 F g^{-1} at 5 A g^{-1} after 1000 cycles, suggesting a promising application in the fabrication of flexible energy storage devices. This work opens up new insights into the design of GS/metal oxide paper as a flexible electrode.

1. Introduction

Up to now, global attention has been paid to various energy-storage devices, such as Li-ion batteries, fuel cells, supercapacitors, *etc.*, due to the ever-increasing energy demands and environmental problems.[1–5] Among them, supercapacitors have shown highly promising applications because of their high power density, low cost, and long cycle life.[6,7] According to the energy storage mechanisms, supercapacitors can be divided into two types.[8] The first one is an electrical double-layer capacitor (EDLC), which involves a non-Faradaic process.[9] The other is a pseudocapacitor, which bears a Faradaic redox reaction for energy storage.[10,11] The specific capacitance of a pseudocapacitor is much higher than that of an EDLC because of the Faradaic redox reaction on the surface of pseudocapacitive materials. Therefore, pseudocapacitive materials, such as NiO,[12] $Ni(OH)_2$,[13] $NiCo_2O_4$,[14] Co_3O_4[15] and MnO_2,[16] which show high specific capacitance, have been widely investigated. The research being conducted towards the abovementioned positive electrode materials (working potential above 0 V *vs.* Hg/HgO) have made great achievements. However, only a few reports on the study of negative electrode materials (working potential below 0 V) have been reported due to their unsatisfying specific capacitance. It is especially important to explore the ideal anode materials, which can match with the cathode materials. Fe_3O_4, with a working potential up to −1 V *vs.* Hg/HgO, has the advantage of easy redox reactions, non-toxicity and low cost. Thus, Fe_3O_4 is considered as one of the most prospective negative electrode materials.

Nevertheless, its poor electrical conductivity leads to slower electron transport rates and less active material availability. These disadvantages cause its poor capacitance of 60–100 F g^{-1}.[17–19] Incorporating conductive materials, such as active carbon,[17] carbon nanotubes[20,21] and graphene,[18,22–24] with Fe_3O_4 to generate composites is a great way to solve the problem of low electrical conductivity. Of all the conductive materials, graphene is superior due to its large surface area (2630 m^2 g^{-1}), high conductivity, and mass production. In addition, the synergistic effects of combining Fe_3O_4 with graphene could considerably improve their electrochemical performance.

Nowadays, only a few studies have been focused on graphene/Fe_3O_4 composites as anode materials for supercapacitors. For example, Qu *et al.*[22] prepared 2D sandwich-like sheets of Fe_3O_4 grown on graphene as high energy anode material and achieved a specific capacitance of 326 F g^{-1} at 0.5 A g^{-1}. Wang and coworkers[24] reported a hydrothermal method for the synthesis of graphene/Fe_3O_4 composites, delivering a capacitance of 220 F g^{-1} at 0.5 A g^{-1} after 3000 cycles. However, working electrodes in the previous reports were prepared by the traditional slurry-coating technology. The electrodes were fabricated by binder and conductive carbon. In fact, the binder will decrease the conductivity of electrode and restrain electron transport, further leading to poor electrochemical performance.

The State Key Lab of High Performance Ceramics and Superfine Microstructure, Shanghai Institute of Ceramics, Chinese Academy of Sciences, 1295 Dingxi Road, Shanghai 200050, P.R. China. E-mail: jingsun@mail.sic.ac.cn; Fax: +86-21-52413122; Tel: +86-21-52414301

† Electronic supplementary information (ESI) available. See DOI: 10.1039/c4ta01442a

Moreover, the conductive carbon hardly contributes to capacitance, while it occupies a certain volume of electrode. The abovementioned reasons hinder the potential applications of graphene/Fe_3O_4 composites in high performance supercapacitors. Therefore, it is highly desirable to design a novel, flexible and binder-free electrode to obtain optimal electrochemical performance.

In this work, a well-organized flexible GS/Fe_3O_4 paper is prepared. Graphene forms a three-dimensional conductive network with homogeneously distributed Fe_3O_4 nanoparticles of ~5 nm. The Fe_3O_4 nanoparticles are grown *in situ* and anchored on graphene sheets by covalent chemical bonding. GS as a flexible confinement material to support Fe_3O_4 nanoparticles prevents the agglomeration of nanoparticles and offers a facile electron transport pathway. Meanwhile, Fe_3O_4 nanoparticles separate GS to avert their restacking, which further increases the interlayer porosity of the paper. Benefiting from the unique 3-D architecture, the flexible GS/Fe_3O_4 paper exhibits excellent rate performance and cyclic stability when compared to traditional electrodes. The optimized GS/Fe_3O_4 paper could achieve a high specific capacitance of 368 F g^{-1} at 1 A g^{-1}, indicating a promising application as a flexible negative electrode. The flexible free-standing paper is expected to play a vital role in fabricating flexible energy-storage devices.

2. Experimental procedure

2.1 Materials preparation

Graphene oxide (GO) was prepared by a modified Hummers method.[25] Then, a certain amount of $Fe(NO_3)_3 \cdot 9H_2O$ was dissolved in 35 mL of DMF, to which 8 mL of a 5 mg mL^{-1} GO suspension was added. The dispersion was continuously stirred at 90 °C for 1 h. The GO/Fe_2O_3 composite paper was obtained by vacuum filtration of the resulting dispersion through a Millipore membrane filter (47 mm in diameter, 0.22 mm in pore size), followed by vacuum drying and peeling off. Finally, the thermal reduction of the GO/Fe_2O_3 composite paper to the desired GS/Fe_3O_4 composite paper was accomplished at 550 °C for 2 h in Ar (Scheme 1). To attain optimal electrochemical performance, the different weight ratios of Fe_3O_4 in GS/Fe_3O_4 were explored. The precursors and obtained products were denoted as GO/Fe_2O_3-1, GO/Fe_2O_3-2, GO/Fe_2O_3-3 and GS/Fe_3O_4-1, GS/Fe_3O_4-2, GS/Fe_3O_4-3. The corresponding Fe_3O_4 contents in the GS/Fe_3O_4 composites are 48.4%, 59.6% and 64.8%. In comparison, pure Fe_3O_4 was prepared by reducing Fe_2O_3 at 350 °C for 1 h in Ar/H_2 (95 : 5).

2.2 Materials characterization

The structures of the products were examined by X-ray power diffraction (XRD) on a Rigaku D/Max-2550V diffractometer using Cu Kα radiation. The morphology of the products was observed on a transmission electron microscope (TEM Tecnai G20 FEI 200 kV) and a scanning electron microscope (SEM JEOL S-4800). Raman spectroscopy was conducted on a DXR Raman Microscope with a 532 nm excitation wavelength. Thermal gravimetric analysis (TGA) was carried out in air at a heating rate of 10 °C min^{-1}. The specific surface area was measured by Brunauer–Emmett–Teller (BET) method at 77 K in N_2 atmosphere using Micromeritics ASAP 2010 surface area analyzer. The conductivity of the GS/Fe_3O_4 composite papers were tested by an Accent HL 5500 at room temperature.

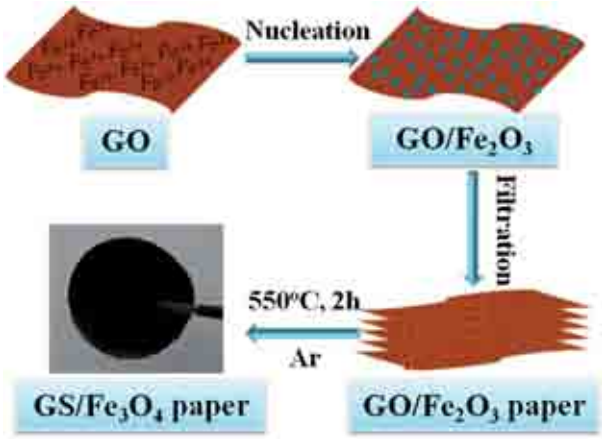

Scheme 1 A schematic illustration of the fabrication processes of the GS/Fe_3O_4 composite paper.

2.3 Electrochemical measurements

The GS/Fe_3O_4 composite papers were used directly as working electrodes without any binder and additive. The GS/Fe_3O_4-3 and Fe_3O_4 traditional electrodes (trad. electrodes) were prepared by slurry-coating technology. Typically, the samples were mixed with acetylene black and polytetrafluoroethylene (PTFE) binder (weight ratio of 8 : 1 : 1) in *N*-methylpyrrolidone (NMP) to form slurries. After stirring uniformly, the slurries were pasted onto a carbon current collector and dried under vacuum at 100 °C for 12 h. All the electrochemical measurements were performed in a three-electrode system. The working electrode was dipped in 1 M KOH aqueous solution. A platinum wire and a Hg/HgO were used as a counter electrode and a reference electrode, respectively. Cyclic voltammetry (CV) measurements were carried out on a Parstat 2273 electrochemical station (Princeton applied research CO., Ltd, USA). Galvanostatic charge–discharge tests were performed on a LAND CT2001A cell 50 measurement system.

3. Results and discussion

The preparation process for GS/Fe_3O_4 composite paper is illustrated in Scheme 1. First, Fe_2O_3 nanoparticles are *in situ* grown and anchored on the surface of GO by covalent chemical bonding. To optimize the GS/Fe_3O_4 composite paper, the precursors (GO/Fe_2O_3) with various iron oxide contents were studied. Fig. 1 shows the TEM images of the GO/Fe_2O_3 composites with different weight ratios. Fe_2O_3 nanoparticles of ~5 nm are homogenously distributed on the GO sheets. However, the pure Fe_2O_3 particles without GO exhibit agglomerated block-shaped structure with irregular large sizes (Fig. S1†). It can be noted that the addition of GO decreases the

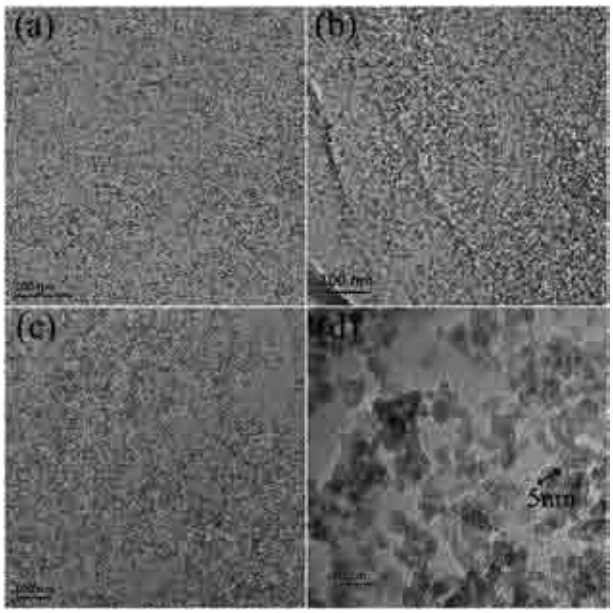

Fig. 1 TEM images of (a) GO/Fe_2O_3-1, (b) GO/Fe_2O_3-2, (c) GO/Fe_2O_3-3, (d) HRTEM image of GO/Fe_2O_3-3.

size and improves the uniformity of the Fe_2O_3 nanoparticles. This is attributed to the dispersing nucleation of Fe^{3+} assisted by the oxygen groups of GO. Moreover, with increasing content of iron source, the Fe_2O_3 nanoparticles on the surface of GO become dense, indicating the increment of Fe_2O_3 content in the GO/Fe_2O_3 composites. After vacuum filtration, flexible GO/Fe_2O_3 composite papers are obtained. Finally, the GO/Fe_2O_3 papers are transformed into GS/Fe_3O_4 papers by simple thermal reduction. Fig. 2 displays the XRD patterns of the GO/Fe_2O_3 and GS/Fe_3O_4 composites. The diffraction peaks of GO/Fe_2O_3 can be assigned to maghemite-c (λ-Fe_2O_3-JCPDS no. 39-1346). After heat treatment, Fe_2O_3 are successfully reduced to Fe_3O_4. All the diffraction peaks are well-indexed to magnetite (Fe_3O_4-JCPDS no. 19-0629), proving that the GS/Fe_3O_4 composites have no other impurity phases. To certify the reduction of GO, Raman spectroscopy (Fig. S2†) of the GO/Fe_2O_3 and GS/Fe_3O_4 composites was recorded. Raman spectra reveals an increasing ratio of D band (~1335 cm^{-1}) to G band (~1589 cm^{-1}) from 1.42 to 1.77. This manifests the reduction of GO, and is in good agreement with previous reports.[26,27] The abovementioned conclusion reveals that the GS/Fe_3O_4 composite is successfully achieved by the reduction of the GO/Fe_2O_3 composite.

Thermogravimetric analysis (TGA) was performed to precisely determine the Fe_3O_4 content in the GS/Fe_3O_4 composite papers. The resulting product is only Fe_2O_3 after TGA, and the corresponding Fe_2O_3 content is 50.1%, 61.7% and 67% for GS/Fe_3O_4-1, GS/Fe_3O_4-2 and GS/Fe_3O_4-3, respectively. Based on the TGA results (Fig. 3), the Fe_3O_4 contents in the GS/Fe_3O_4 composites are calculated to be 48.4%, 59.6% and 64.8%. The iron oxide content increases gradually, which is consistent with the results of TEM. The weight ratio of GS and Fe_3O_4 would influence the specific surface area of the composite. Fig. 4 represents the nitrogen adsorption/desorption isotherms of the GS/Fe_3O_4 composites with different weight ratios. The specific surface areas are 346.1, 323.1 and 310 m^2 g^{-1} for GS/Fe_3O_4-1, GS/Fe_3O_4-2 and GS/Fe_3O_4-3, respectively. Hence, with the reduction of graphene content, the specific surface area of GS/Fe_3O_4 composite decreases. It is reasonable because GS with larger specific surface area could provide more surface area in the composites.[28–30] Moreover, the GS/Fe_3O_4 composites in this work possess a much larger specific surface area than those reported previously.[29–32] Furthermore, the GS/Fe_3O_4 composites exhibit type IV nitrogen adsorption–desorption isotherms, indicating the presence of mesopores. Specifically, the pore sizes are 3–4 nm calculated by the BJH method from the pore size distribution plots. As is well-known, the large specific surface area and suitable pore size distribution in the range of 2–5 nm is favorable for electrochemical reactions[33,34] because the large specific surface areas can provide the high availability of electrode materials. Meanwhile, appropriate pore size facilitates better diffusion and accession of electrolyte ions through pore channels for efficient redox reactions during the charge storage process.

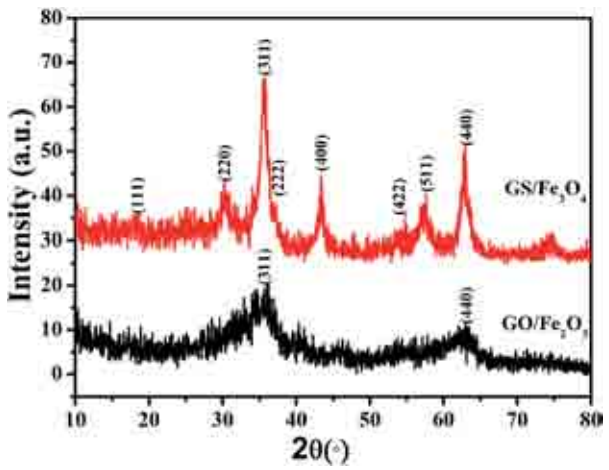

Fig. 2 XRD patterns of GO/Fe_2O_3 and GS/Fe_3O_4 composites.

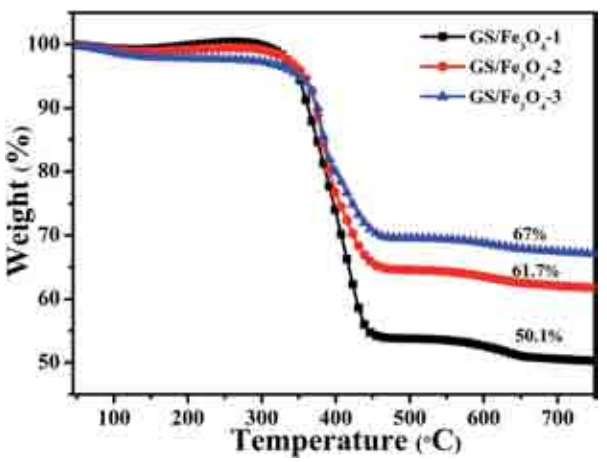

Fig. 3 TG profiles of GS/Fe_3O_4 composites with different weight ratios.

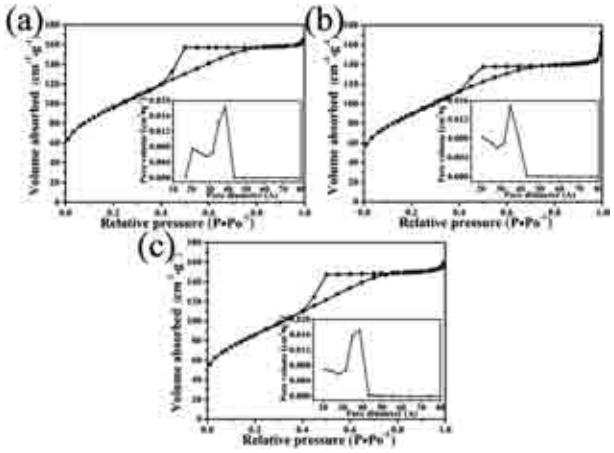

Fig. 4 Nitrogen adsorption–desorption isotherms (with the BJH pore size distributions plots in the insets.) measured at 77 K for (a) GS/Fe_3O_4-1, (b) GS/Fe_3O_4-2, (c) GS/Fe_3O_4-3.

From this viewpoint, the GS/Fe_3O_4 composite papers could be used as excellent negative electrode materials.

To characterize the composite paper in detail, TEM and SEM of GS/Fe_3O_4-3 paper were further investigated. From the top-view images (Fig. 5a), the Fe_3O_4 nanoparticles are uniformly anchored on the surface of GS without any aggregates. The cross-sectional image discloses the 3-D layered structure of the GS/Fe_3O_4-3 paper with a thickness of ~8.88 μm (Fig. 5b). To further observe the inner morphology, TEM images are given in Fig. 5c and d. Fe_3O_4 nanoparticles of ~5 nm are homogeneously dispersed on the surface of the GS. The inset of Fig. 5c shows the selected-area electron diffraction (SAED) pattern. The rings index to the (220), (311), and (400) planes of Fe_3O_4, which is in accordance with the XRD data. The HRTEM image (Fig. 5d) reveals a lattice distance of 0.297 nm, corresponding to the (220) plane of Fe_3O_4. In the 3-D layered structure, GS improves the dispersion of Fe_3O_4 nanoparticles, while Fe_3O_4 prevents the agglomeration of GS. Therefore, the unique structure facilitates electron transport, further boosting the accessible capacity of the GS/Fe_3O_4-3 paper electrode.

To confirm the best mass ratio of the GS/Fe_3O_4 papers as negative electrodes, the electrochemical performance of the GS/Fe_3O_4 papers with different Fe_3O_4 contents were evaluated by cyclic voltammetry and galvanostatic charge–discharge. The CV measurements of the GS/Fe_3O_4 composite papers (Fig. 6a) were recorded at 5 mV s^{-1} in the potential range of −1–0 V. The width of the CV curves decreases in the order of GS/Fe_3O_4-3 > GS/Fe_3O_4-2 > GS/Fe_3O_4-1, demonstrating the reduction of specific capacitance in this sequence. To evaluate this in detail, galvanostatic charge–discharge measurements of the GS/Fe_3O_4 composite papers were carried out at various current densities in a potential window of −1–0 V. The specific capacitance was calculated from the corresponding galvanostatic discharge curves (Fig. 6b–d) according to the following equation:

$$C_s = \frac{I\Delta t}{m\Delta V}$$

where C_s is the specific capacitance, I is the current density, m is the mass of active materials in the electrode, and V is the voltage difference. As determined in Fig. 6e, the GS/Fe_3O_4-3 paper shows much better capacitance performance when compared with the others at all the current densities. The specific

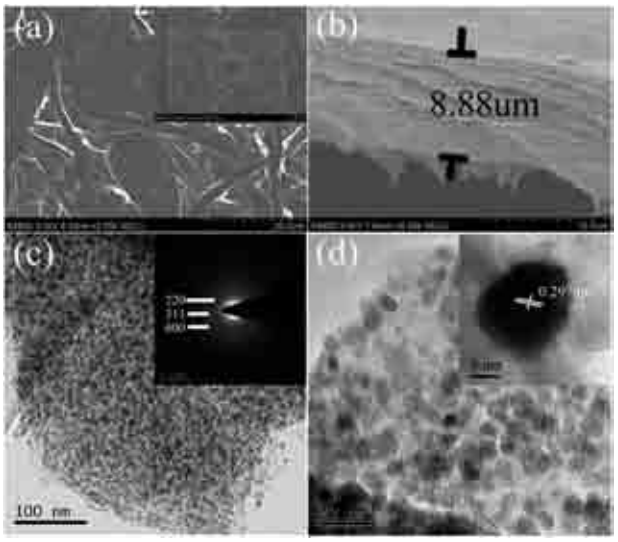

Fig. 5 (a) Top-view SEM images of GS/Fe_3O_4-3 composite paper. (b) Cross-sectional SEM image of GS/Fe_3O_4-3 composite paper. (c) TEM image of GS/Fe_3O_4-3 composite. (d) HRTEM images of GS/Fe_3O_4-3 composite.

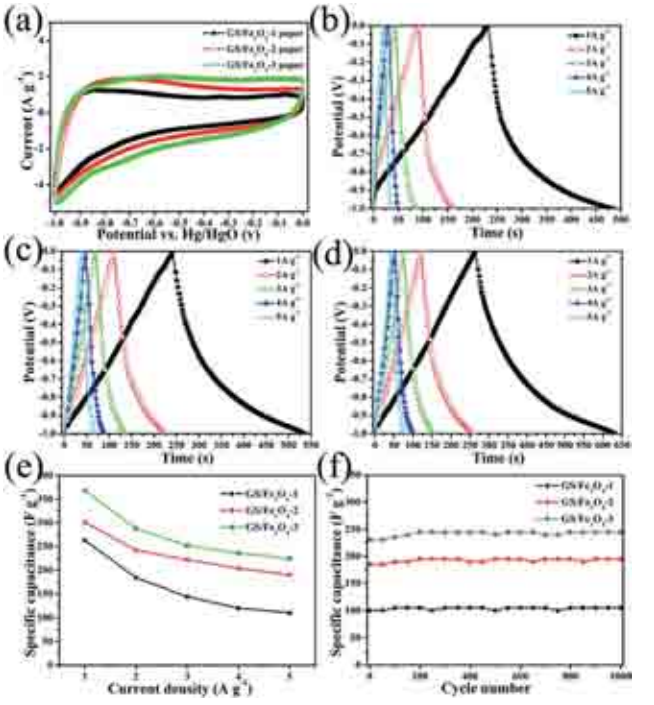

Fig. 6 Electrochemical characterization of GS/Fe_3O_4 composite papers: (a) CV curves at a scan rate of 5 mV s^{-1}. Galvanostatic charge–discharge curves of GS/Fe_3O_4-1 (b) GS/Fe_3O_4-2 (c) GS/Fe_3O_4-3 (d) at different current densities. (e) Average specific capacitance at different current densities. (f) Cyclic performance at 5 A g^{-1}.

capacitance of GS/Fe_3O_4-3 paper is calculated to be 368 F g^{-1} at a current density of 1 A g^{-1} based on the total mass of the paper. However, the capacitance of the GS/Fe_3O_4-1 and GS/Fe_3O_4-2 papers gradually decreases to 263 and 301 F g^{-1}, respectively, which are both poorer than the GS/Fe_3O_4-3 paper. In addition, the GS/Fe_3O_4-3 paper possesses a large specific capacitance of 225 F g^{-1} even at a high current density of 5 A g^{-1}. After the 1000-cycle test at 5 A g^{-1} (Fig. 6f), the specific capacitance of the GS/Fe_3O_4-3 paper is still as high as 245 F g^{-1}, suggesting excellent cyclic performance. It is worth noting that the GS/Fe_3O_4-3 paper presents optimized performance when compared with the GS/Fe_3O_4-1 and GS/Fe_3O_4-2 papers at all current densities, and is consistent with the conclusion of the CV testing. We can explore why the GS/Fe_3O_4-3 paper displays the best performance from its physical properties (Table 1). For electrode materials, the specific surface area, mass ratio of active materials, and conductivity are generally crucial for specific capacitance. In this study, from GS/Fe_3O_4-1 to GS/Fe_3O_4-2 and GS/Fe_3O_4-3, the content of GS decreases gradually, leading to the reduction of their specific surface areas and conductivities. The two factors are unfavorable for specific capacitance. While the mass ratio of Fe_3O_4 as the active material increases gradually, which may offer more Faradaic redox reaction, further enhance the specific capacitance. This is reasonable because even in the GS/Fe_3O_4-3 composite, we can see that Fe_3O_4 nanoparticles of ~5 nm are monodispersed on the surface of GS from the TEM image. The Fe_3O_4 content is not enough to cover the GS. Therefore, GS/Fe_3O_4-3, with the most Fe_3O_4 content, possesses the maximum contact points between graphene and Fe_3O_4 nanoparticles, as shown in Scheme 2. Apparently, the specific surface area and conductivity of the three GS/Fe_3O_4 papers changes slightly; therefore, Fe_3O_4 content influences more significantly. Therefore, the comprehensive effect of three factors is that GS/Fe_3O_4-3 exhibits optimal electrochemical performance.

To highlight the advantages of the unique 3-D GS/Fe_3O_4-3 paper as a negative electrode, the conventional electrodes of Fe_3O_4 and GS/Fe_3O_4-3 (with 10 wt% acetylene black, 10 wt% PTFE binder, and 80 wt% active material) were prepared by slurry-coating technology, which are denoted as Trad. Fe_3O_4 and Trad. GS/Fe_3O_4, respectively. From the CV curves (Fig. 7a), we can easily figure out that the capacitance of the GS/Fe_3O_4-3 paper is much higher than those of Trad. Fe_3O_4 and Trad. GS/Fe_3O_4. In addition, Trad. GS/Fe_3O_4 has a better performance compared to Trad. Fe_3O_4. Futhermore, galvanostatic charge–discharge measurements were performed to further study their electrochemical performance (Fig. S3†). Fig. 7b indicates the

Table 1 Physical properties of GS/Fe_3O_4 papers

Samples	Fe_3O_4 contents	Specific surface area (m^2 g^{-1})	Resistivity (ohm $square^{-1}$)
GS/Fe_3O_4-1	48.4	346.1	14.5
GS/Fe_3O_4-2	59.6	323.1	16.9
GS/Fe_3O_4-3	64.8	310	20.2

Scheme 2 A schematic illustration of the GS/Fe_3O_4 composites with different Fe_3O_4 content.

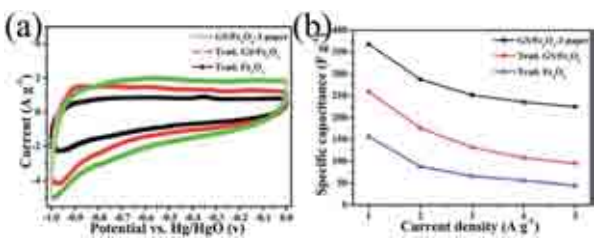

Fig. 7 (a) CV curves of the GS/Fe_3O_4-3 paper, Trad. GS/Fe_3O_4 and trad. Fe_3O_4 at a scan rate of 5 mV s^{-1}. (b) Average specific capacitance at different current densities.

average specific capacitance calculated from the galvanostatic discharge curves at different current densities. The specific capacitance values of the GS/Fe_3O_4-3 paper are 368, 288, 252, 236, and 225 F g^{-1} at 1, 2, 3, 4 and 5 A g^{-1}, respectively. For Trad. Fe_3O_4 and Trad. GS/Fe_3O_4, the values are 157, 88, 66, 56, 45 and 260, 176, 132, 108, 95 F g^{-1}, respectively. Moreover, the GS/Fe_3O_4-3 paper possesses a specific capacitance of 225 Fg^{-1} at a high current density of 5 A g^{-1}, which is ~61.1% of that at 1 A g^{-1}. While for Trad. Fe_3O_4 and Trad. GS/Fe_3O_4, the corresponding capacitance retention is 28.7% and 36.5%, respectively. In addition, the specific capacitance values stabilize at 245, 95 and 45 Fg^{-1} for the GS/Fe_3O_4-3 paper, Trad. GS/Fe_3O_4 and Trad. Fe_3O_4 after 1000 cycles, respectively. Evidently, the GS/Fe_3O_4-3 paper possesses the best capacitance and rate performance, followed by Trad. GS/Fe_3O_4, and Trad. Fe_3O_4 is the worst.

The superior performance of the GS/Fe_3O_4-3 paper can be attributed to the following reasons. (i) As a flexible confinement material to support Fe_3O_4 nanoparticles, the GS prevents the agglomeration of the Fe_3O_4 nanoparticles. Thus, it increases their effective availability and improves the accessible capacitance. (ii) GS provides good electrical contact and paves a route for electron transport, further boosting the rate performance and cycle stability. and (iii) the Fe_3O_4 nanoparticles separate GS and prevent restacking, providing better immersion and diffusion of the electrolyte ions through pore channels for efficient redox reactions during the charge storage process. These three reasons explain that the introduction of GS can promote the electrochemical performance, further verifying that there are more advantages with GS/Fe_3O_4-3 paper and Trad. GS/Fe_3O_4 than Trad. Fe_3O_4 as a supercapacitor. When compared with Trad. GS/Fe_3O_4, the GS/Fe_3O_4-3 paper has its own unique merits. First, the flexible paper acts as an electrode and avoids the addition of an electrically insulating polymer binder, which promotes the charge transfer rate. Second, GS offers a

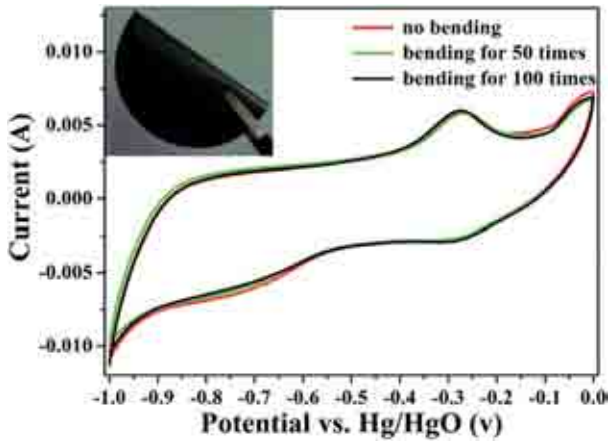

Fig. 8 The CV cycles of the GS/Fe_3O_4-3 paper at different bending times (The inset is the digital photo of GS/Fe_3O_4-3 paper.).

continuous conductive network to efficiently decrease the particle–particle interface resistance, improving the availability of the Fe_3O_4 during redox reactions. Third the interlayer spacing of the paper facilitates electrolyte ions transportation. Therefore, this unique layered GS/Fe_3O_4-3 paper can dramatically improve cycling stability and rate capability of Fe_3O_4 as an anode material for supercapacitors.

As is well-known, the mechanical flexibility and bending properties of the paper electrode are significant because they are critical for device assembly. To prove the mechanical flexibility of GS/Fe_3O_4-3, the CV curves of GS/Fe_3O_4-3 paper were measured at different bending times. As shown in Fig. 8, after the paper electrode was bended for 50 and 100 times, the CV curves are almost identical with those with no bending. There is no capacitance loss after bending, which further proves that the GS/Fe_3O_4 paper is a prospective candidate as a flexible supercapacitor.

4. Conclusion

In summary, a three-step approach is presented for the construction of flexible GS/Fe_3O_4 composite paper. Fe_3O_4 nanoparticles of ~5 nm are uniformly grown *in situ* and anchored on the surface of GS by covalent chemical bonding. The graphene sheet simultaneously functions as a conductive agent and binder. Rapid charge transport from the Fe_3O_4 nanoparticles to the underlying graphene provides efficient redox reactions. The optimized GS/Fe_3O_4 paper (64.8%) exhibits excellent rate performance and cyclic stability. It could achieve a high specific capacitance of 368 F g^{-1} at 1 A g^{-1}, and 225 F g^{-1} at 5 A g^{-1}, making the GS/Fe_3O_4 paper a promising candidate for a flexible negative electrode material. This work opens up a universal and economic strategy to fabricate other GS/metal oxide composite papers for flexible energy-storage devices.

Acknowledgements

This work is supported by the National Basic Research Program of China (2012CB932303), the National Natural Science Foundation of China (Grant no. 51172261) and the supportion from the committee of Shanghai Science and Technology (13XD1403900).

References

1 K. Fu, O. Yildiz, H. Bhanushali, Y. X. Wang, K. Stano, L. G. Xue, X. W. Zhang and P. D. Bradford, *Adv. Mater.*, 2013, **25**, 5109–5114.
2 B. Koo, H. Xiong, M. D. Slater, V. B. Prakapenka, M. Balasubramanian, P. Podsiadlo, C. S. Johnson, T. Rajh and E. V. Shevchenko, *Nano Lett.*, 2012, **12**, 2429–2435.
3 H. Chang, S. H. Joo and C. Pak, *J. Mater. Chem.*, 2007, **17**, 3078–3088.
4 X. Y. Lang, A. Hirata, T. Fujita and M. W. Chen, *Nat. Nanotechnol.*, 2011, **6**, 232–236.
5 H. Jiang, P. S. Lee and C. Z. Li, *Energy Environ. Sci.*, 2013, **6**, 41–53.
6 Z. J. Fan, J. Yan, T. Wei, L. J. Zhi, G. Q. Ning, T. Y. Li and F. Wei, *Adv. Funct. Mater.*, 2011, **21**, 2366–2375.
7 L. F. Chen, Z. H. Huang, H. W. Liang, W. T. Yao, Z. Y. Yua and S. H. Yu, *Energy Environ. Sci.*, 2013, **6**, 3331–3338.
8 G. P. Wang, L. Zhang and J. J. Zhang, *Chem. Soc. Rev.*, 2012, **41**, 797–828.
9 K. Xie, X. T. Qin, X. Z. Wang, Y. N. Wang, H. S. Tao, Q. Wu, L. J. Yang and Z. Hu, *Adv. Mater.*, 2012, **24**, 347–352.
10 G. H. Yu, L. B. Hu, N. Liu, H. L. Wang, M. Vosgueritchian, Y. Yang, Y. Cui and Z. N. Bao, *Nano Lett.*, 2011, **11**, 4438–4442.
11 H. Jiang, J. Ma and C. Z. Li, *Adv. Mater.*, 2012, **24**, 4197–4202.
12 C. Y. Cao, W. Guo, Z. M. Cui, W. G. Song and W. Cai, *J. Mater. Chem.*, 2011, **21**, 3204–3209.
13 H. L. Wang, H. S. Casalongue, Y. Y. Liang and H. J. Dai, *J. Am. Chem. Soc.*, 2010, **132**, 7472–7477.
14 T. Y. Wei, C. H. Chen, H. C. Chien, S. Y. Lu and C. C. Hu, *Adv. Mater.*, 2010, **22**, 347–351.
15 C. C. Xiang, M. Li, M. J.Zhi, A. Manivannan and N. Q. Wu, *J. Power Sources*, 2013, **226**, 65–70.
16 L. Mao, K. Zhang, H. S. O. Chan and J. S. Wu, *J. Mater. Chem.*, 2012, **22**, 1845–1851.
17 X. Du, C. Y. Wang, M. M. Chen, Y. Jiao and J. Wang, *J. Phys. Chem. C*, 2009, **113**, 2643–2646.
18 W. H. Shi, J. X. Zhu, D. H. Sim, Y. Y. Tay, Z. Y. Lu, X. J. Zhang, Y. Sharma, M. Srinivasan, H. Zhang, H. H. Hng and Q. Y. Yan, *J. Mater. Chem.*, 2011, **21**, 3422–3427.
19 L. Wang, H. M. Ji, S. S. Wang, L. J. Kong, X. F. Jiang and G. Yang, *Nanoscale*, 2013, **5**, 3793–3799.
20 A. B. Deshmukh and M. V. Shelke, *RSC Adv.*, 2013, **3**, 21390–21393.
21 Y. H. Kim and S. J. Park, *Curr. Appl. Phys.*, 2011, **11**, 462–466.
22 Q. T. Qu, S. B. Yang and X. L. Feng, *Adv. Mater.*, 2011, **23**, 5574–5580.
23 J. P. Cheng, Q. L. Shou, J. S. Wu, F. Liu, V. P. Dravid and X. B. Zhang, *J. Electroanal. Chem.*, 2013, **698**, 1–8.
24 Q. H. Wang, L. F. Jiao, H. M. Du, Y. J. Wang and H. T. Yuan, *J. Power Sources*, 2014, **245**, 101–106.

25 W. S. Hummers and R. E. Offeman, *J. Am. Chem. Soc.*, 1958, **80**, 1339.
26 Z. Gao, J. Wang, Z. Li, W. Yang, B. Wang, M. Hou, Y. He, Q. Liu, T. Mann, P. Yang, M. Zhang and L. Liu, *Chem. Mater.*, 2011, **23**, 3509–3516.
27 J. Chang, H. Xu and J. Sun, *J. Mater. Chem.*, 2012, **22**, 11146–11150.
28 X. L. Yang, K. C. Fan, Y. H. Zhu, J. H. Shen, X. Jiang, P. Zhao and C. Z. Li, *J. Mater. Chem.*, 2012, **22**, 17278–17283.
29 G. M. Zhou, D. W. Wang, F. Li, L. L. Zhang, N. Li, Z. S. Wu, L. Wen, G. Q. Lu and H. M. Cheng, *Chem. Mater.*, 2010, **22**, 5306–5313.
30 F. Zhang, T. F. Zhang, X. Yang, L. Zhang, K. Leng, Y. Huang and Y. S. Chen, *Energy Environ. Sci.*, 2013, **6**, 1623–1632.
31 R. H. Wang, C. H. Xu, J. Sun, L. Gao and C. C. Lin, *J. Mater. Chem. A*, 2013, **1**, 1794–1800.
32 J. Su, M. H. Cao, L. Ren and C. W. Hu, *J. Phys. Chem. C*, 2011, **115**, 14469–14477.
33 X. J. Zhang, W. H. Shi, J. X. Zhu, W. Y. Zhao, J. Ma, S. Mhaisalkar, T. L. Maria, Y. H. Yang, H. Zhang, H. H. Hng and Q. Y. Yan, *Nano Res.*, 2010, **3**, 643–652.
34 P. Simon and Y. Gogotsi, *Nat. Mater.*, 2008, **7**, 845–854.